PROCEEDINGS OF SPIE

SPIEDigitalLibrary.org/conference-proceedings-of-spie

Optical coherence tomography characterization of femtosecond laser manufactured microfluidic circuits

Lucas Ramos De Pretto, Ricardo Elgul Samad, Wagner de Rossi, Anderson Zanardi de Freitas

Lucas Ramos De Pretto, Ricardo Elgul Samad, Wagner de Rossi, Anderson Zanardi de Freitas, "Optical coherence tomography characterization of femtosecond laser manufactured microfluidic circuits," Proc. SPIE 10491, Microfluidics, BioMEMS, and Medical Microsystems XVI, 104911A (19 February 2018); doi: 10.1117/12.2289937

SPIE.

Event: SPIE BiOS, 2018, San Francisco, California, United States

Optical coherence tomography characterization of femtosecond laser manufactured microfluidic circuits

Lucas Ramos De Pretto, Ricardo Elgul Samad, Wagner de Rossi and Anderson Zanardi de Freitas*
Nuclear and Energy Research Institute, IPEN-CNEN/SP, Avenida Lineu Prestes, 2242, Cidade Universitária São Paulo - SP –Brasil CEP 05508-000

ABSTRACT

Dimensional characterization of microfluidic circuits were performed using three-dimensional models constructed from OCT images of such circuits. Were fabricated microchannels on the same BK7 glass plate, under different laser ablation conditions and substrate displacement velocity in relation to laser beam. Were used the following combination of energy, from 30 μJ to 60 μJ and velocity from 588 mm/min to 1176 mm/min, at 1 kHz laser repetition rate and 40 fs of pulse duration (FWHM). For OCT imaging we used an OCP930SR (Thorlabs System Inc) with 930 nm central wavelength, 6 μm of lateral and axial resolution, and image of 500 x 512 pixel corresponding to 2.0 mm x 1.6 mm of lateral and axial scans respectively at 8 frames per second. We also characterized devices like, micropumps, microvalves and microreactors. It was possible register the micropumps and valves in action in real time. Using the OCT images analyses was possible to select the best combination of laser pulse energy and substrate velocity. All the devices were made in raster protocol, where laser beam pass through the same path in a controlled number of times, and with each iteration more material is removed and deeper the channels remain. We found a deformation at the edge of fabricated structures, due to velocity reduction of substrate in relation to laser beam, which causes more laser pulses superposition in these regions, and more material is ablated. The technique was thus evaluated as a potential tool to aid in the inspection of microchannels.

Keywords: Optical coherence tomography, microfluidics, femto second laser manufacturing.

1. INTRODUCTION

Optical Coherence Tomography (OCT)[1] is a noninvasive, contactless imaging technique based on white-light interferometry that generates high resolution, cross-sectional images of scattering media. These images provide morphological information about internal structures of samples. The micrometer-resolution, aligned with its penetration depth places OCT in an unique spot among other imaging modalities[2,3,4].

Microfluidics is currently an area of great research growth. Such interest is justified by the variety of applications the technique makes possible in areas such as optics, biology, chemistry, and electronics. It is characterized, therefore, as a powerful tool that still explores its limits, with the advances in the manufacture of microfluidic components. Since its origin, derived from other techniques such as capillary electrophoresis[5], these microfluidic devices have already witnessed various manufacturing techniques, with varied materials as a basis and rapid technological advances, motivated even for military applications. The complexity of microfluidic systems also grows, on the one hand, the new possibilities of machining and, on the other, the requirements of new experiments that sometimes require several chemical reactions in the same component. This is the trend of the so-called "lab-on-a-chip" LOC[6]. These devices give rise to the miniaturization and automation of various types of processes and chemical reactions, adding an enormous potential, proven by the existence of magazine dedicated exclusively to LOC. From microreactors to chemical syntheses, to portable tools for optical diagnosis, such as to do cytometry and check the blood leucocyte density[7], applications dependent on this type of system become more frequent.

*freitas.az@ipen.br; phone: +55 11 3133 9356; www.ipen.br

Microfluidics, BioMEMS, and Medical Microsystems XVI, edited by Bonnie L. Gray, Holger Becker, Proc. of SPIE Vol. 10491, 104911A · © 2018 SPIE · CCC code: 1605-7422/18/$18 · doi: 10.1117/12.2289937

However, in order for the microfluidic components to meet demand in a satisfactory manner, it is essential that the manufacture, in particular of the microchannels, be made properly. In this sense, it is important that there are methods to verify and characterize the manufactured structures, so that it is possible to be sure of the quality of the microchannel

produced. Several techniques are employed for this purpose, among which SEM (Scanning Electron Microscopy) stands out. However interferometric techniques are also applied, among them the OCT[8].

Our group has already demonstrated the ability not only to produce microchannels from femtosecond laser ablation, but also to analyze them through our OCT systems. This opens up a range of microfluidic study options, including volumetric flow determination[9]. This characterization is important as feedback for the production of the microchannels, besides assuring the quality for use in experiments and gathering data concerning them.

.

2. MATERIAL AND METHODS

All experiments described in this work were performed using the Optical Coherence Tomography system - OCP930SR (Thorlabs Inc.), with a central wavelength at 930 nm, and spatial resolution of 6.0 μm (lateral and axial) in air; with image up to 2000x515 pixels ; In this system the commercial data acquisition software provided with the equipment was used.

For the first study, eight microchannels were fabricated on the same BK7 glass plate, under different ablation conditions, as follows, in Table 1, where E is the energy per pulse of the laser, and V is the rate of displacement of the substrate. We used 1 kHz laser repetition rate, 40 fs of pulse duration (FWHM), a focalization lens of f=38 mm provinding a spotsize of d=15 μm at surface substrate.

Table 1. Parameters of interest used in the manufacture of microchannels

#	E (μJ)	V (mm/min.)
1	30	1176
2	30	588
3	60	1176
4	60	1176
5	60	588
6	60	1176
7	60	588
8	60	349

A photo of these microchannels can be found in Figure 1.

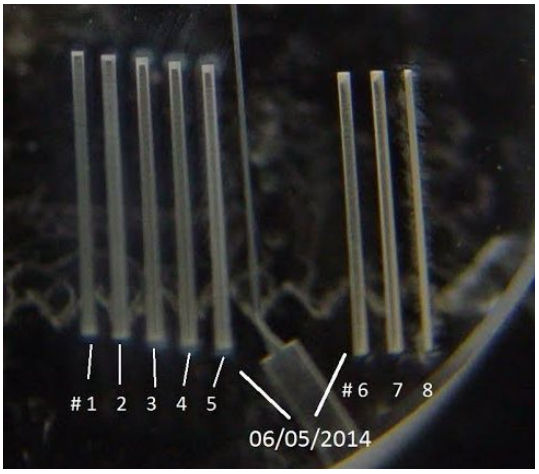

Figure 1. Microchannels studied.

To perform the measurements, the OCT system was used with image size of 512 pixels (axial) x 500 pixels (lateral) corresponding to 1.58 mm (axial) x 2.0 mm (lateral). With this lateral coverage it was not possible to sample all the microchannels in a single image, for this reason, the microchannels were divided into groups so that all the channels of a given group fit into a single image. The first group comprises channels 1 to 3, the second group with microchannels 4 and 5, leaving 6 to 8 for the third and last group. An example of the image of group 2 is in Figure 2. The images for the other groups are similar.

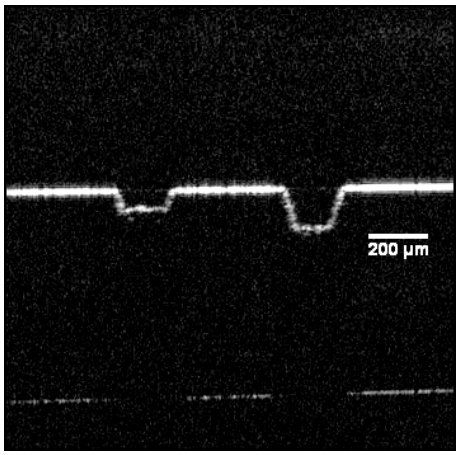

Figure 2. Example of OCT image of group 2, with microchannels 4 (left) and 5 (right).

In order to evaluate the uniformity and obtain more precise data on the microchannels, an analysis was performed in several locations of the microchannels, along their longitudinal extension. For this, the sample was placed on an automated MT3-Z8 linear translator (Thorlabs Inc.). By controlling the speed and distance of sample displacement, a 3 mm scan was performed on each channel, simultaneously obtaining OCT images with the same characteristics as in Figure 2, at a rate of 8.6 fps (frames per second), which allowed the subsequent three-dimensional channels reconstruction, with a longitudinal resolution (along the microchannel) of 5.0 µm.

The physical measurements were made in fifteen different locations of each microchannel, with the first being always at the beginning of these. After this, the measurement was separated by 148 µm (or 30 frames), covering a surface range of approximately 2.08 mm. Three-dimensional reconstruction was done with the VGStudioMax® software, and Figure 3 shows an example of obtained results.

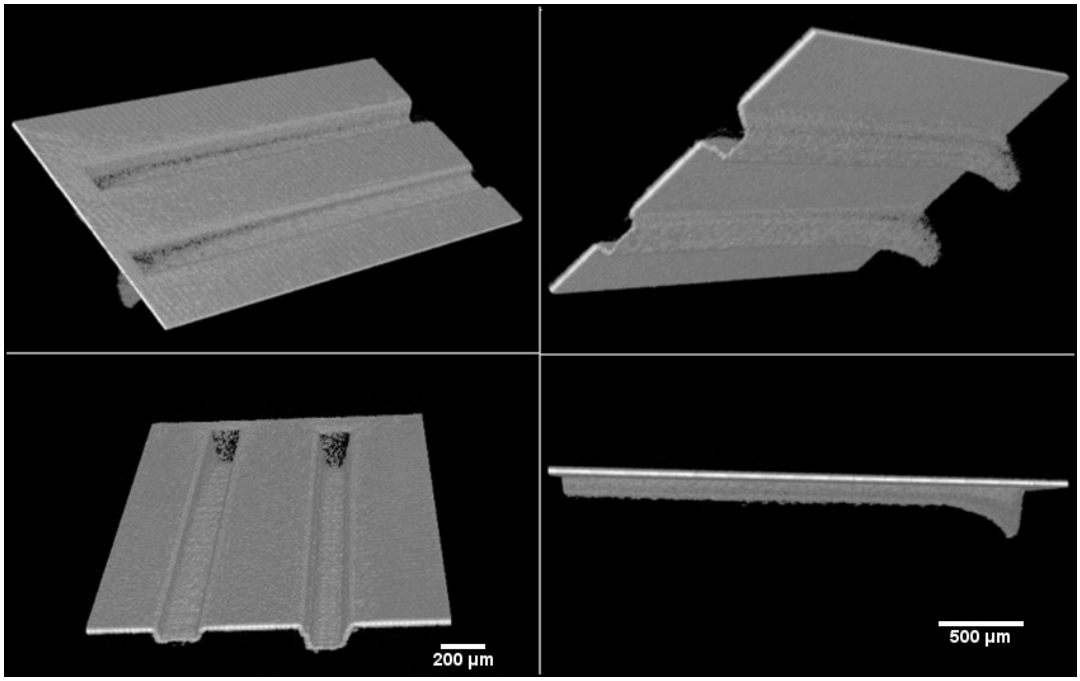

Figure 3. 3D reconstruction of the channels of group 2, under different viewing angles

The VGStudioMax® software also has measurement tools for analyzing three-dimensional volume data. Through these tools, and calibrating the software with the acquisition parameters, we characterized the physical dimensions of the microchannels.

3. RESULTS AND DISCUSSION

3.1 Microchannels

The first feature to be noted is the deformation at the ends of the fabricated structures. As can be seen in the Figure 3, there is a huge depression in the channels as they approach the edge. This is true for all eight microchannels, and is due to the manufacturing process through the pulsed laser.

In machining these circuits, the substrate used for ablation is displaced in a longitudinal direction, while the laser beam is fixed, which allows it to scan the surface of the substrate. When it reaches a certain length, the sample undergoes a small lateral displacement, and a new sweep begins in the opposite longitudinal direction. This lateral displacement is necessary to control the width of the microchannel, and is repeated until the necessary extension is reached, concatenating a longitudinal displacement with one side, completing a movement called raster. The next raster starts, causing the laser beam to pass through the same path previously described. This cycle is repeated by a controlled number of times, and with each iteration more material is removed from the structure, and deeper the channels remain. However, whenever scanning approaches a longitudinal limit, there is a reduction in the velocity of displacement of the substrate, which causes more laser pulses to concentrate in these regions, and more material is ablated. For this reason, the ends of the channels become deeper and more irregular than the rest.

Thus, one of the analyzes carried out was the depth of the channels, in which results the aberration at the evaluated end is clearly perceived. These results are contained in the graph of Figure 4.

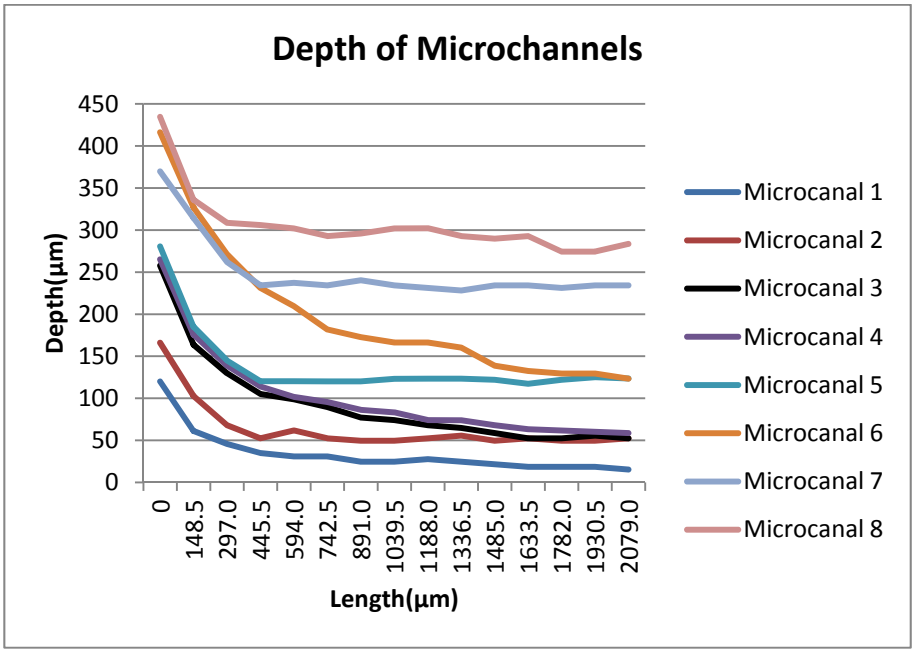

Figure 4. Comparative chart of the depth of the 8 microchannels as a function of length

The mean and standard deviation, presented in Table 2, consider all measurements, including those performed at the extremities, which influence the calculation of these values, and may not be good indicators of the quality of microfluidic circuits. For comparison, the mean and standard deviation were recalculated, taking into account only the measurements outside the depression zone, from 445.5 µm away from the end. These new results are also shown in Table 2 .

Table 2. Mean and Standard Deviation of the depth along the microchannels. Overall Values consider the full extent, while Recalculated Values take into account from 445.5µm from microchannels end. All values in microns.

Microchannels	Average overall	Standard deviation	Averege recalculated	Standard Deviation recalculated
1	34.56	26.49	24.27	6.01
2	64.2	31.28	52.29	3.56
3	93.37	55.54	70.78	18.55
4	101.34	55.80	78.39	17.99
5	138.06	42.90	121.73	2.14
6	197.04	83.57	161.80	33.86
7	250.26	39.47	233.99	3.07
8	305.81	38.60	292.34	10.47

The values obtained without the zone of depression are more in agreement with what was observed of the microchannels during the measurements, in a matter of uniformity.

However, one can observe in Figure 4 that in half of the channels □ numbers 1, 3, 4 and 6 □ there was a constant decrease of depth along the microchannel. Especially noteworthy in the number 1 microchannel, which already had a

smaller depth than the others, and becomes even shallower, being only 15 µm from surface. When analyzing the configuration parameters, it is verified that they are precisely the machined channels with a greater speed of displacement, indicating that a very fast sweep can generate less uniform structures. In addition, channel number 1, manufactured with a lower power, suffered more with this factor. This measurements was done out of optimised lasers and displacement conditions, presenting standard deviation higher than normal for laser ablation, and this parameter was utilized as feedback for optimization processes.

A similar analysis was made for the width of the channels. Measurements were also performed at fifteen different sites of the microchannels. The width was measured at the opening of the microchannels, on the surface. As can be seen from the values in Figure 5, the manufacturing problems are not repeated in this analysis, and the small variations of the values occur in a similar way throughout the length. As the result is similar for all channels, the parameters used for the machining do not have a great influence on the variations presented along the microchannel.

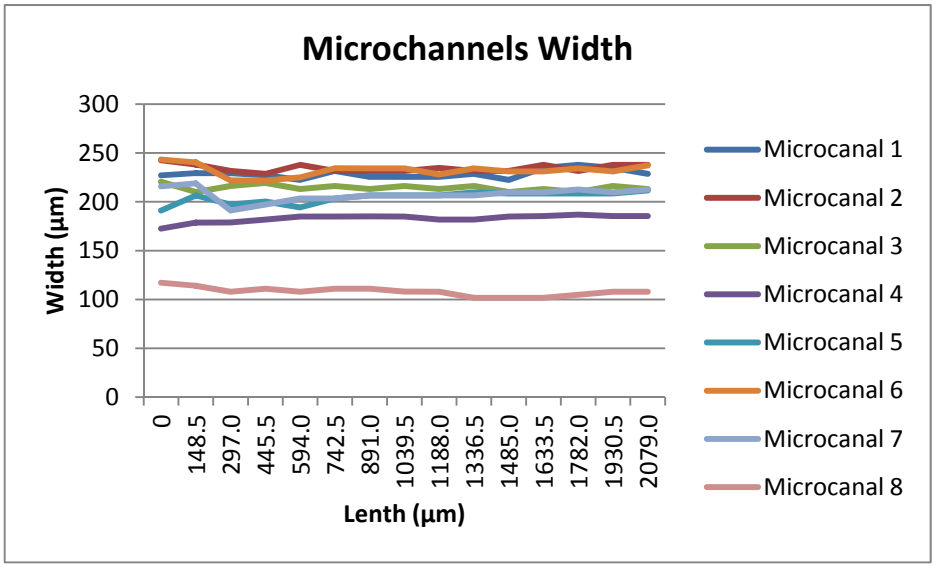

Figure 5. Comparative graph of the width at the opening of the 8 microchannels as a function of length

There are differences between the average width values between microchannels, but they do not present an apparent relation with the manufacturing parameters studied.

The fluctuation of values along the same microchannel may result from that the beam at a certain depth still ablates material of smaller depths (surface), which makes the structure less uniform. This factor also contributes to the fact that the channels do not present a regular profile along their entire depth. The internal angles of its walls are not perfectly straight, causing the width to change from depth to depth, and an analysis of the aperture at the surface would not properly characterize the structures.

Were carried therefore also analyzes the width and half the depth of the base of each channel. These two new procedures were also repeated in ifteen different locations. The results are Figure 6 and Figure 7. Again, calculated the mean and standard deviation, including and excluding the depression region, as shown in Table 3.

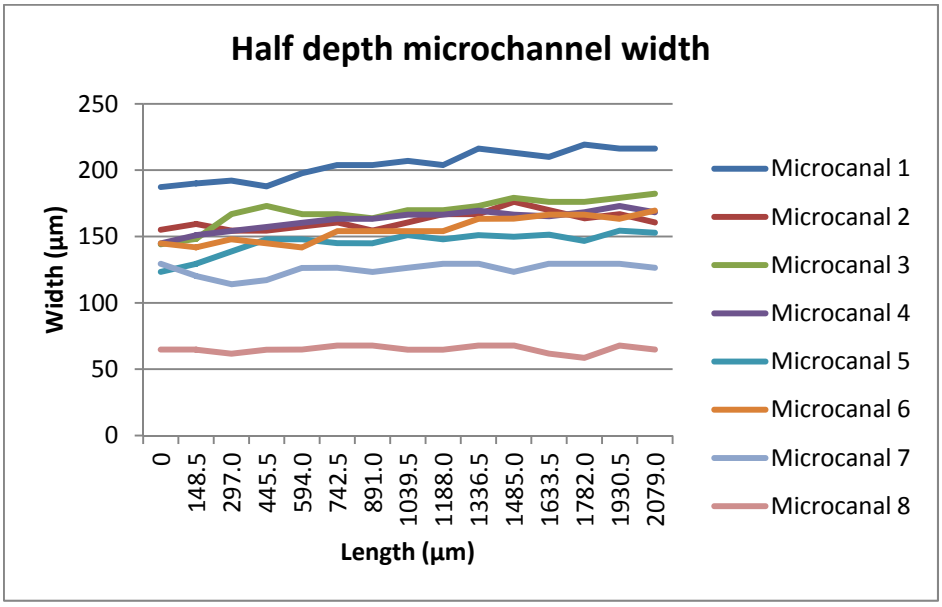

Figure 6. Comparative graph of the width at half height of the 8 microchannels as a function of length

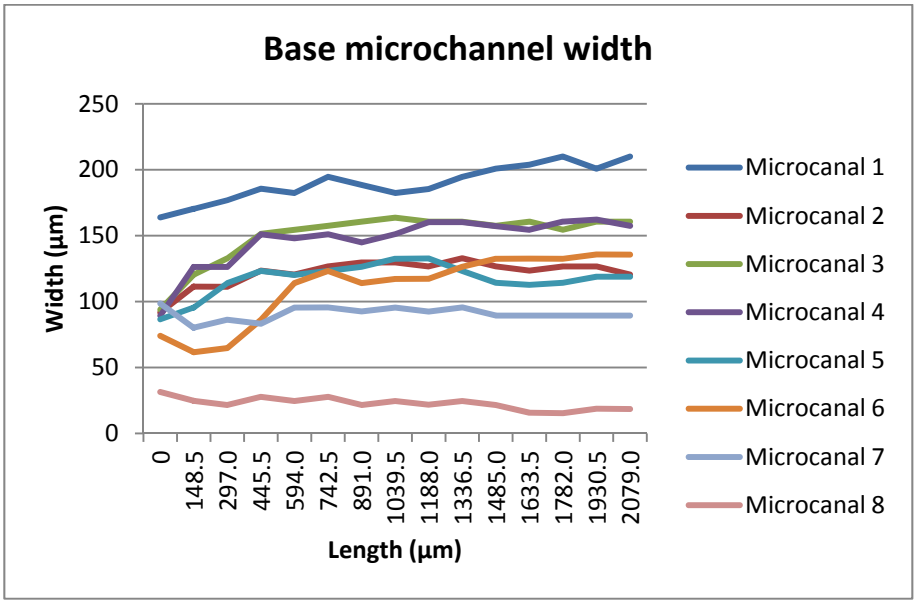

Figure 7. Comparative graph of the width at the base of the 8 microchannels as a function of length.

Table 3. Width mean and standard deviation along microchannels, at half depth and at base. Average consider the full extent, while Average recalculated take into account from 445.5µm, like previosly. All values in µm

	Half depth microchannel width			
Microchannels	Average	Standard Deviation	Average Recalculated	Standard Deviation Recalculated
1	204.31	11.09	207.93	9.17

2	161.81	6.45	163.19	6.42
3	168.99	10.70	172.97	5.73
4	162.52	7.68	165.65	4.21
5	145.48	8.72	149.23	3.02
6	155.33	9.60	157.95	8.83
7	125.33	4.90	126.37	3.72
8	64.94	2.72	65.25	2.89
	Width at base			
	Average	**Standard deviation**	**Average recalculated**	**Standard deviation recalculated**
1	**189.99**	**13.82**	**194.90**	**10.19**
2	**121.85**	**10.33**	**126.12**	**3.68**
3	**149.99**	**19.51**	**158.56**	**3.56**
4	**146.71**	**19.39**	**154.88**	**5.62**
5	**117.12**	**12.37**	**121.73**	**6.56**
6	**111.18**	**26.25**	**122.28**	**14.06**
7	**90.82**	**5.06**	**91.44**	**3.79**
8	**22.69**	**4.49**	**21.89**	**4.19**

This time, the effects of the greater number of pulses at the extremities are visible, especially in the measurements in microchannels base. The measurements show the average at hal depth slightly narrower results at the end of the microchannel and an enlargement tendency to move away from the edge, while measures at the microchannels base have significantly smaller values at this location. This confirms what could be visually attested in the three-dimensional reconstruction of Figure 3: in the regions of depression, the channel acquires a more triangular profile, so the base becomes much smaller than its aperture at the surface. This result indicates that the end-of-course aberration not only deforms the depth of the microchannel, but also its profile.

Exceptions to the mentioned case are channels 7 and 8. As can be seen from the results in Figure 7, the width differences at the beginning and along these structures are not expressive as in most cases. In microchannel 7, the explanation is a manufacturing defect. One of the inner walls of the channel has a protuberance, and ends up narrowing the inner passage, as can be seen in Figure 8 on the left . For channel 8, the results obtained are due to the fact that the channel as a whole has a more triangular profile, also shown to the right in Figure 8, which indicates that the manufacturing parameters, combining a high power and low scan speed may not be appropriate for some experiments requiring square-profile channels. This also corroborates the aberrations explanation at the ends of the microstructures, where the same situation occurs: slower speed and higher deposited energy (more pulses).

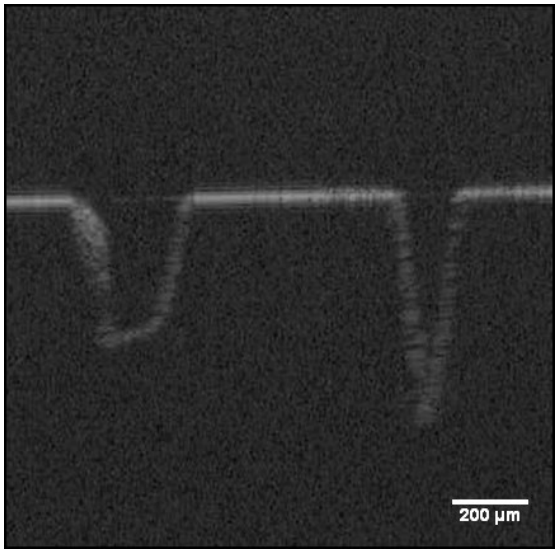

Figure 8. Detail of the microchannels 7 (left) and 8 (right).

Such a triangular profile, different from the others, is a result of the combination of sharp angles of the internal walls and great depth. To confirm this, measurements of the angles of the internal walls were carried out in relation to the base of the microchannels. For each of these, the angles were measured at five different locations, spaced 0.495 mm apart, the first measurement being performed at the end of the microchannel. Results are presented in Table 4.

Table 4. Internal wall angles of the channels relative to the base. DP indicates the standard deviation. General values consider the full extent, while Recalculated Values take into account from 495 µm.

#	Wall	Start	495 µm	990 µm	1485 µm	1980 µm	Average	SD	Average Rec.	SD Rec.
1	left (°)	108.44	127.69	122.28	123.02	126.87	121.66	7.75	124.97	2.71
	right (°)	109.9	127.87	132.27	146.98	143.75	132.15	14.73	137.72	9.11
2	left (°)	115.96	140.01	141.58	143.75	144.9	137.24	12.05	142.56	2.19
	right (°)	112.22	142.35	143.5	146.69	146.93	138.34	14.73	144.87	2.29
3	left (°)	102.86	108.85	111.45	117.65	115.35	111.23	5.79	113.33	3.93
	right (°)	101.71	113.38	120.65	118.44	126.87	116.21	9.44	119.84	5.59
4	left (°)	100.47	106.56	103.45	105.95	109.55	105.20	3.42	106.38	2.51
	right (°)	101.12	107.45	113.61	113.43	114.23	109.97	5.66	112.18	3.17
5	left (°)	101.16	109.65	110.41	108.36	110.56	108.03	3.94	109.75	1.01
	right (°)	101.92	109.89	109.8	109.01	110.88	108.30	3.63	109.90	0.77
6	left (°)	102.09	103.85	104.53	105.83	107.59	104.78	2.07	105.45	1.65
	right (°)	102.99	108.23	109.66	109.3	111.63	108.36	3.25	109.71	1.42

7	left (°)	102.99	102.53	101.31	95.71	96.23	99.75	3.51	98.95	3.48
	right (°)	101.85	104.21	104.71	105.75	107.63	104.83	2.12	105.58	1.51
8	left (°)	96.14	99.27	99.37	98.29	98.93	98.40	1.33	98.97	0.49
	right (°)	98.5	99.65	98.75	98.05	98.51	98.69	0.59	98.74	0.67

It is clear that the internal angles of channel 8 are more pronounced than the others, which makes it a particular case, and explains the difference of it to the remaining microchannels. In addition, it is possible to verify that in the first measurement site (at the beginning of the channels) the measured angles in all cases also become more accentuated. This, together with the depth information of Figure 4, justifies the difference noted in the microchannel profile in the depression regions.

It is also worth noting the behavior of the left wall angles of channel 7. These decrease as they move away from the end, contrary to what is observed for the remaining cases. Again, this is caused by the protrusion on this inner wall.

The results obtained with OCT were compared with other results, measured through optical profiling, a higher resolution technique. The profilometer used was ZeGage Profiler (Zygo Corporation). It was found that the values obtained with both techniques were compatible, as shown in Figure 9 and Figure 10, analyzes of the number 4 microchannel, respectively measuring depth and width at the base. In Figure 9 the parameter Rdz is highlighted , which indicates the height difference between the horizontal dotted lines. In Figure 10, the highlighted parameter is Rdx, indicating the distance between the solid vertical lines. This proof of the measures enables the OCT as a potential tool for analyzing the quality of microchannels.

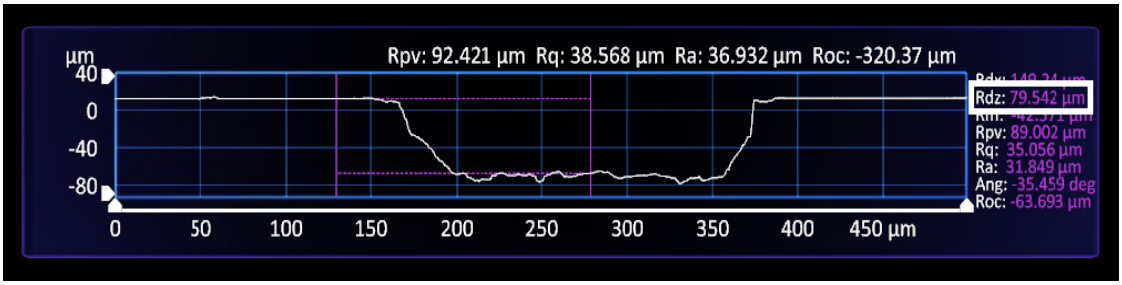

Figure 9. Measurement of optical profilometry for the depth of the microchannel number 4.

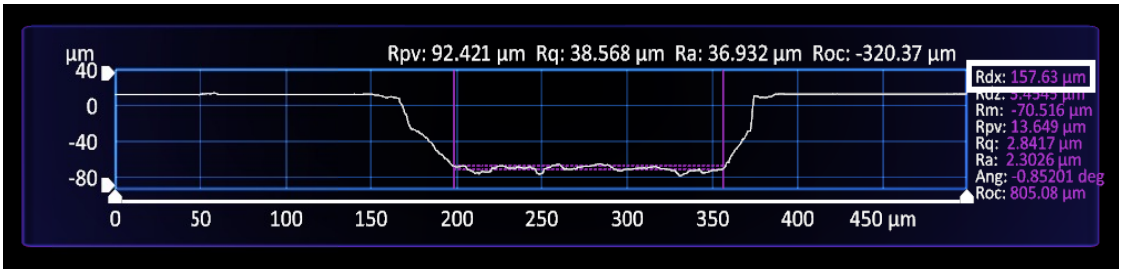

Figure 10. Measurement of optical profilometry for the width of microchannel number 4

3.2 Microvalves and micropumps

We also developed some microvalve, that was characterized with OCT in real time. A movie can be seen in Figure 11.

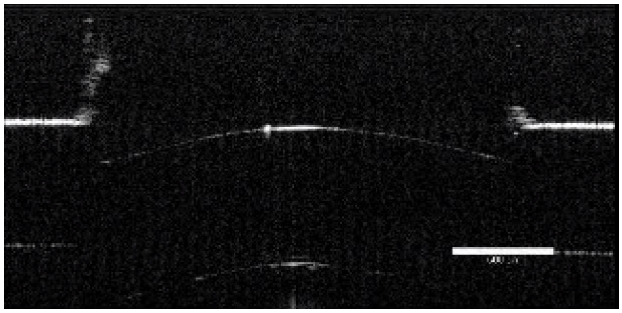

Figure 11. Valve_ON_OFF.wmv, OCT in real time during ON/OFF valve operation, http://dx.doi.org/doi.number.goes.here

And in a Figure 12, a 3D reconstruction of valve, showing its components

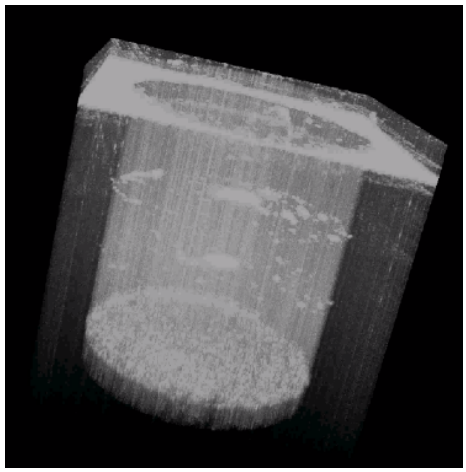

Figure 12. 3d_movie_valve.wmv, OCT 3D valve recontruction, http://dx.doi.org/doi.number.goes.here

4. CONCLUSIONS

In this work, the ability and applicability of the OCT to carry out evaluations of the physical dimensions of microfluidic circuits was verified.

In this way, it was possible to analyze important aspects of the microchannels in different manufacturing conditions. These measures serve as feedback to the ablation process and allow us to gain some intuition about the result to be expected for parameters of interest in the machining of these structures. In addition, knowledge of the physical dimensions of the channels is essential for the calculation of various other properties of such microfluidic devices, such as flow, for example.

For the present study, the most important result is the demonstration of OCT as an adequate tool to control the quality of these microfluidic devices. In addition, these tests served as an operating instruction for commercial OCT systems, and provided a solid foundation for further testing.

5. ACKNOWLEDGEMENT.

The authors would like to thanks the grant # 449440/2014-1, National Council for Scientific and Technological Development (CNPq) and grant # 2013/26113-6, São Paulo Research Foundation (FAPESP)

REFERENCES

[1] D. Huang, E. A. Swanson, C. P. Lin, J. S. Schuman, W. G. Stinson, W. Chang, M. R. Hee, T. Flotte, K. Gregory, C. A. Puliafito, J. G. Fujimoto, "Optical coherence tomography," Science 254, 1178 (1991).
[2] W. Drexler, and J. G. Fujimoto, "Optical Coherence Tomography: Technology and Applications", Springer, (2008).
[3] E. Sattler, R. Kästle, and J. Welzel, "Optical coherence tomography in dermatology," J. Biomed. Opt. 18, 061224-1 (2013).
[4] A. M. Zysk, F. T. Nguyen, A. L. Oldenburg, D. L. Marks, and S. A. Boppart, "Optical coherence tomography: a review of clinical development from bench to bedside," J. Biomed. Opt. 12, 051403-1 (2007).
[5] WHITESIDES, GM., "The origins and the future of microfluidics," Nature 442, 368 (2006)
[6] JENSEN, KF; REIZMAN, BJ; NEWMAN, "SG Tools for chemical synthesis in microsystems," Lab on a Chip 14, 3206 (2014)
[7] ZHU, HY et al. "Optofluidic Fluorescent Imaging Cytometry on a Cell Phone," Analytical Chemistry 83, 6641 (2011)
[8] MACHADO, LM et al. "Microchannels Direct Machining using the Femtosecond Smooth Ablation Method," Lasers in Manufacturing 2011: Proceedings of the Sixth International Wlt Conference on Lasers in Manufacturing 12, 67 (2011)
[9] L. R. De Pretto, G. E. C. Nogueira, and A. Z. Freitas, "Microfluidic volumetric flow determination using optical coherence tomography speckle: An autocorrelation approach," J. of Applied Physics 119, 163105 (2016)